Journal of Power Sources 206 (2012) 497–503

Contents lists available at ScienceDirect

Journal of Power Sources

journal homepage: www.elsevier.com/locate/jpowsour

# Evaluation of carbon composite materials for the negative electrode in the zinc–cerium redox flow cell

Georgios Nikiforidis[a], Léonard Berlouis[a,*], David Hall[b], David Hodgson[b]

[a] WestCHEM, Department of Pure and Applied Chemistry, University of Strathclyde, Glasgow G1 1XL, UK
[b] Plurion Ltd., Glenrothes, Fife KY6 2TF, UK

ARTICLE INFO

*Article history:*
Received 31 August 2010
Received in revised form
10 November 2010
Accepted 13 January 2011
Available online 21 January 2011

*Keywords:*
Redox flow batteries
Zinc–cerium
Carbon substrates
Methane sulfonic acid

ABSTRACT

An investigation into the suitability of three carbon composites as substrates for the negative electrode in the zinc–cerium redox flow cell has been carried out. The composite electrodes examined comprised the use of polyvinylidene fluoride (PVDF) and high density polyethylene (HDPE) as binders for the carbon and the third was a graphite foil electrode of ~1 mm thickness. The zinc deposition process was carried out in a methane sulfonic acid (MSA) electrolyte at 60 °C and nucleation studies revealed the growth of the deposits to be instantaneous in this medium. Galvanostatic charge/discharge cycles were performed in order to test the performance of these composite materials under a variety of operating conditions. For all the materials, the highest charge/discharge coulombic efficiencies (~95%) were found for the highest discharge current densities (200 mA $cm^{-2}$) employed in the study but this falls as the charge period is increased. The effect of solution flow velocity is however less clear. Prolonged zinc charging–discharging cycling on the composite materials revealed that whereas the PVDF-based electrode exhibited no loss in efficiency with cycling (>250), a drastic reduction was observed for the HDPE-based and graphite foil electrodes beyond 70 cycles and this was accompanied by the physical deterioration in the electrode surface.

© 2011 Elsevier B.V. All rights reserved.

## 1. Introduction

Redox flow batteries are a class of reversible energy storage systems in which the active materials of the battery, in both charged and discharged state, are soluble. As this allows the active material to be stored externally to the battery system itself, the energy of the redox battery can thus be determined independently of the battery power because it is related to the electrolyte volume whereas the power is related to the electrode size. In normal operation, the charged reactants are circulated through the cell stack, consisting of the electrodes and/or separators, causing spontaneous discharge of the different reactive species at the anode and the cathode. Several systems have been examined over the last two decades, including the vanadium–vanadium [1–3] bromine–polysulfide [4,5], iron–chromium [6–8] and vanadium–bromine flow [9] batteries. Many of these have achieved pilot-scale operations as well as being commercially exploited [10–15]. Reviews of the different flow cell technologies have been carried by Bartolozzi [16] and Ponce de Léon et al. [17]. In essence therefore, the electrodes themselves serve only as an electrical interface for the transfer of ionic to electronic current through the cell. In practice however, the nature and form of these electrode materials and surfaces play a very big role in the coulombic, voltage and energy efficiencies obtained for the redox flow cells as well as in repeated cycling stability. In redox flow cells where one of the electrode reactions involves the deposition of a metallic species, such as in the zinc–bromine [18–20], zinc–chlorine [21] and the soluble lead acid batteries [22,23], then the issue of the form of the metallic deposit and self-discharge rates become very important considerations in the design of such systems [24]. These so-called redox flow hybrid systems have been widely studied and are already available commercially [25,26].

The zinc/cerium flow cell, developed by Plurion Ltd. [27], is a recent introduction to this field. At the negative electrode during charging, the metal ions move from the solution and deposit onto the inert carbon substrate ($Zn^{2+} + 2e^- \rightarrow Zn$) whereas at the positive electrode, oxidation of the $Ce^{3+}$ to $Ce^{4+}$ occurs at a noble metal or alloy electrode. The anolyte here consists of 6.9 M $CH_3SO_3H$ MSA and 1.5 M ZnO and 0.4 M $Ce_2(CO_3)_3{\cdot}6H_2O$. The catholyte is 0.4 M $Ce_2(CO_3)_3{\cdot}6H_2O$ in 6.9 MSA and 0.9 M ZnO, the latter to reduce loss of the anode active material to the catholyte side. The presence

☆ This paper is based on work presented at the International Flow Battery Forum, 15 & 16 June 2010. The aim of the International Flow Battery Forum is to encourage the discussion and dissemination of information relating to the research, development, demonstration, manufacture and operation of flow battery components and systems.

* Corresponding author at: University of Strathclyde, Department of Pure and Applied Chemistry, Thomas Graham Building, 295 Cathedral Street, Glasgow G1 1XL, UK. Tel.: +44 141 548 4244; fax: +44 141 548 4822.
*E-mail address:* l.berlouis@strath.ac.uk (L. Berlouis).

0378-7753/$ – see front matter © 2011 Elsevier B.V. All rights reserved.
doi:10.1016/j.jpowsour.2011.01.036

of the cerium in the solution at the negative electrode reaction does not affect the zinc deposition reaction and although it was sometimes omitted from the prepared solutions, the change in ionic strength of the solution had little impact on the results obtained. The cell is operated at 60 °C and the open circuit voltage is ~2.5 V, which is nearly double of that of other cells. Key in achieving this is the high solubility of the cerium and of the zinc in the organic acid. MSA has also been employed as an electrolyte for the electrodeposition of tin, copper and tin–copper alloys [28] as well as being the electrolyte of choice in soluble lead acid batteries [23].

In this paper, we concentrate solely on the negative electrode side of the Zn/Ce cell and investigate the Zn deposition/dissolution process on a number of carbon plastic electrodes. Cyclic voltammetry, potential step and rotating disk (RDE) studies as well as multiple galvanostatic charge/discharge cycles were employed in order to evaluate the effectiveness, robustness and so potential use of three carbon composite materials in this redox flow cell.

## 2. Experimental details

The composite carbon samples used in this study are essentially carbon material compacted and held together by a polymer resin. The first of these, referred to as Type I in the text, uses polyvinylidene fluoride (PVDF) as the binder and is commonly employed as carbon bipolar plates in the proton exchange membrane fuel cell. The second, referred to as Type II, employs high density polyethylene, (HDPE) giving good thermal and electrical conductivity. The third carbon material examined, referred to as Type III, was a graphite foil electrode of ~1 mm thickness. Finally, a glassy carbon (Alfa Aesar) electrode was also employed for comparison purposes. For the electrochemical studies, these materials were cut into cylinders of suitable diameter which could be mounted onto an Oxford Electrodes® rotating disc electrode set up and sealed flush with the external surface. Apart from rinsing of the carbon surface with ethanol prior to first use, care was taken to ensure that the samples did not suffer any mechanical damage to the exposed surface. For the glassy carbon electrode used for comparison of the electrochemical behaviour of these composite materials, mechanical polishing of its surface was carried out using a polishing cloth with 0.3 μm alumina powder (Buehler). A standard 3-electrode configuration was employed, with a platinum gauze acting as the counter electrode and the reference electrode was a $Hg|Hg_2SO_4|K_2SO_4$ (sat.), which has a potential of 0.64 V vs. the normal hydrogen electrode. The electrolyte was contained in a jacketed cell which enabled its temperature to be controlled (±1 °C) by means of a thermostatted water bath (Gallenkamp thermostirrer 95). All solutions were prepared using Milli-Q deionised water (resistivity 18.2 MΩ cm) using methyl sulfonic acid (70%, BASF), ZnO (99.5%, Fisher Chemicals), cerium carbonate (20 wt% $H_2O$, Zibo Jiahua Advanced Material Resources Ltd.) and anhydrous sodium carbonate (99.8%, GPR).

The cyclic votammograms and the potential step studies were carried out using an EG & G M100A Potentiostat/Galvanostat controlled by custom written software in LabVIEW. The scan rate employed for all the cyclic voltammograms was 20 mV $s^{-1}$ between the potential limits of 0.2 V and −2 V. For the galvanostatic charge/discharge cycles, a Solartron 1260 Electrochemical Interface controlled by Corrware® software was employed. The morphology of the electrodeposits and of the composite carbon surfaces following repeated cycling experiments were examined using SEM (Cambridge Instruments Spectroscan 90).

## 3. Results and discussion

The cyclic voltammogram of the zinc deposition from a solution of 10 mM $Zn^{2+}$ in 0.25 M $Na(CH_3SO_3)$ at 27 °C is shown in Fig. 1.

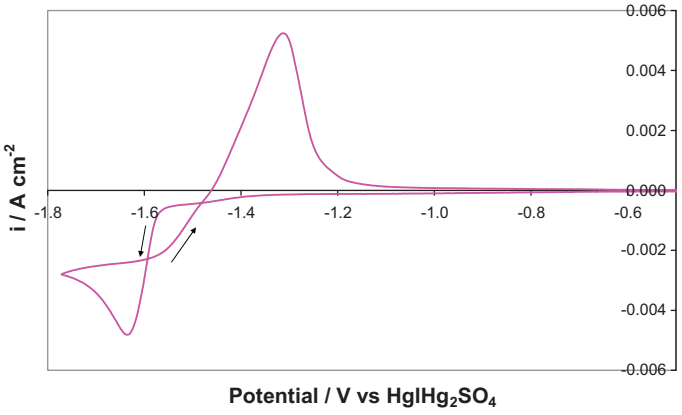


**Fig. 1.** Cyclic voltammogram of Type I (PVDF) electrode in $1.0 \times 10^{-2}$ M $Zn^{2+}$ and 0.25 M $Na(CH_3SO_3)$ at 60 °C; scan rate = 20 mV $s^{-1}$.

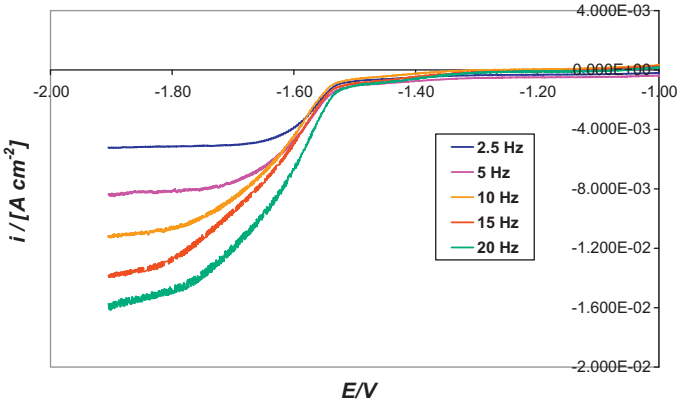


**Fig. 2.** Rotating disc electrode study of Type II (HDPE) in $1.0 \times 10^{-2}$ M $Zn^{2+}$ and 0.25 M $Na(CH_3SO_3)$ at 60 °C; scan rate = 10 mV $s^{-1}$.

This shows an onset for deposition at −1.58 V with a diffusion-controlled deposition peak at −1.68 V. The classic nucleation loop indicates the formation of a new phase onto the Type I (PVDF) electrode surface. The zinc dissolution process leads to a very symmetrical peak, characteristic of a surface-controlled process. The data from a rotating disc electrode (RDE) study on the deposition process is shown in Fig. 2. Through the use of the Levich equation [29] the diffusion coefficients of the zinc-methylsulphonate species at three different temperatures, viz. 27 °C, 40 °C and 60 °C indicated were determined in this system. The RDE study also allowed the standard rate constant for the electron transfer process to be obtained and compared for the different carbon-based materials employed in this study. The latter was derived from the examination of the current at potentials in the mixed control region. Through the use of the Koutechy–Levich relationship [30,31]

$$\frac{1}{i} = \frac{1}{0.62nFD^{2/3}\nu^{-1/6}C\omega^{1/2}} + \frac{1}{nFkC} \quad (1)$$

where $\omega$ is the angular rotation frequency (rad $s^{-1}$) and $\nu$ is the kinematic viscosity of the solution, the rate constant $k$ at a given potential in the mixed controlled region can be obtained, and from which, the standard rate constant $k^o$ can be evaluated. The resulting analyses from the RDE study is given in Table 1. The values obtained for the diffusion coefficient are in accordance with the literature values [32] and as expected, increase with temperature. Likewise, the standard rate constants evaluated also increase with temperature with the Type II based carbon composite showing the slightly faster kinetics compared to the Type I (PVDF) or GC electrodes.

**Table 1**
Rate constants and diffusion coefficients obtained as a function of temperature from the RDE in $1.0 \times 10^{-2}$ M $Zn^{2+}$ and 0.25 M $Na(CH_3SO_3)$.

| Temperature (°C) | $10^3 \times k^o$ (cm s$^{-1}$) | | | $10^5 \times D$ (cm$^2$ s$^{-1}$) |
|---|---|---|---|---|
| | Glassy carbon | Type I (PVDF) | Type II (HDPE) | |
| 27 | 0.16 | 0.69 | 1.57 | 0.69 |
| 40 | 0.32 | 1.16 | 1.64 | 0.98 |
| 60 | 0.97 | 2.32 | 3.4 | 1.35 |

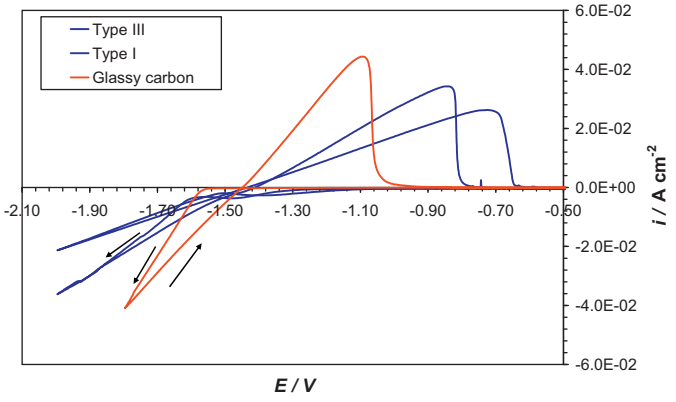


**Fig. 3.** Cyclic voltammograms of the different carbon electrodes in 1.5 M $Zn^{2+}$ in 0.4 M $Ce_2(CO_3)_3{\cdot}6H_2O$ and 6.9 M $CH_3SO_3H$ at 60 °C; scan rate = 20 mV s$^{-1}$.

The cyclic voltammograms carried out in 6.9 M MSA containing 1.4 M $Zn^{2+}$ on these three electrodes are shown in Fig. 3. The onset for the zinc deposition process is significantly lower (by *ca.* 100 mV) for the Type III (foil) electrode compared to PVDF one. However, the deposition rate and hence, amount deposited during the cathodic scan, is much greater for the PVDF and GC electrodes Indeed, the rate of growth of the zinc layer at the GC surface is the fastest of the three electrode materials examined and this can be attributed to the different resistivities of the carbon materials. No diffusion peak is present over the potential range examined as the deposition is inevitably accompanied by the hydrogen evolution reaction (HER) at the more negative potentials. The latter process is however inhibited on the electrodeposited zinc surface, as can be gleaned from the exchange current density values for the HER on zinc which is only $3.16 \times 10^{-11}$ A cm$^{-2}$ [33]. A nucleation loop is again evident here and the dissolution of the electrodeposited layer yields the characteristic curve for a surface controlled reaction and also shows that the process is delayed and appears much slower in the case of the Type III foil and Type I PVDF electrodes compared to the GC.

One essential feature of any electrodeposition process (and certainly the case here) is the formation and growth of nuclei of the new phase onto the inert substrate. The three-dimensional nucleation and growth of the centres is commonly analysed in terms of either instantaneous, where all the nuclei are formed simultaneously or progressive, where the nuclei are formed at different times during the growth process, resulting in growth centres that are different in size. In the former, the number of nuclei formed depends on the energy provided for the growth, *i.e.*, the applied overpotential and in the latter, an added factor is the rate constant for formation of new nuclei which also increases with potential. It is important to note that the compactness and physical stability of the layer grown will depend not only on the adherence of the deposit to the substrate but also on the number of nuclei formed and the rate of evolution of these growth centres. In order to derive such information, a study was carried out in which the potential was stepped from a region where no growth occurs to increasing values of potential sufficient to initiate the growth of the electrodeposits. The *I*–*t* transients recorded from such a study in $1.0 \times 10^{-2}$ M $Zn^{2+}$ and 0.25 M $Na(CH_3SO_3)$ are shown in Fig. 4 for the Type I (PVDF) carbon electrode. As expected, this shows that with increasing negative potential, the current maximum increases and occurs at shorter times. The analysis of these curves was carried out according to the method of Scharifker et al. [34,35] in which the normalised current (with respect to the maximum current $I_m$) is plotted against the normalised time, where $t_m$ is the time at which $I_m$ occurs. This is shown in Fig. 5 for two potentials and it can be clearly seen that of the two nucleation and growth mechanisms examined here, that for instantaneous nucleation is a far better fit to the experimental

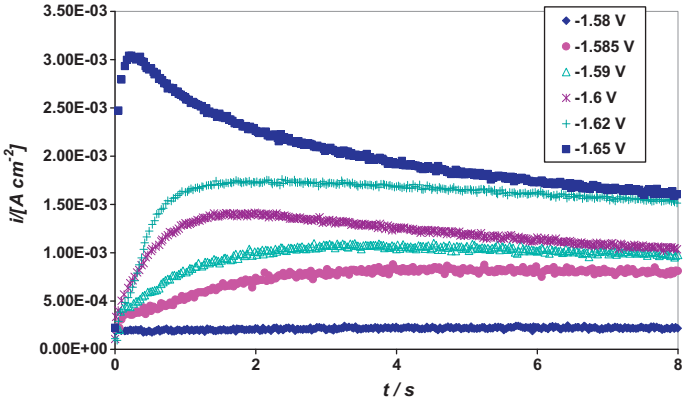


**Fig. 4.** *I*–*t* transients recorded for potential step experiments in 0.25 M $Na(CH_3SO_3)$ at 27 °C on Type I (PVDF) containing $5 \times 10^{-3}$ M $Zn^{2+}$.

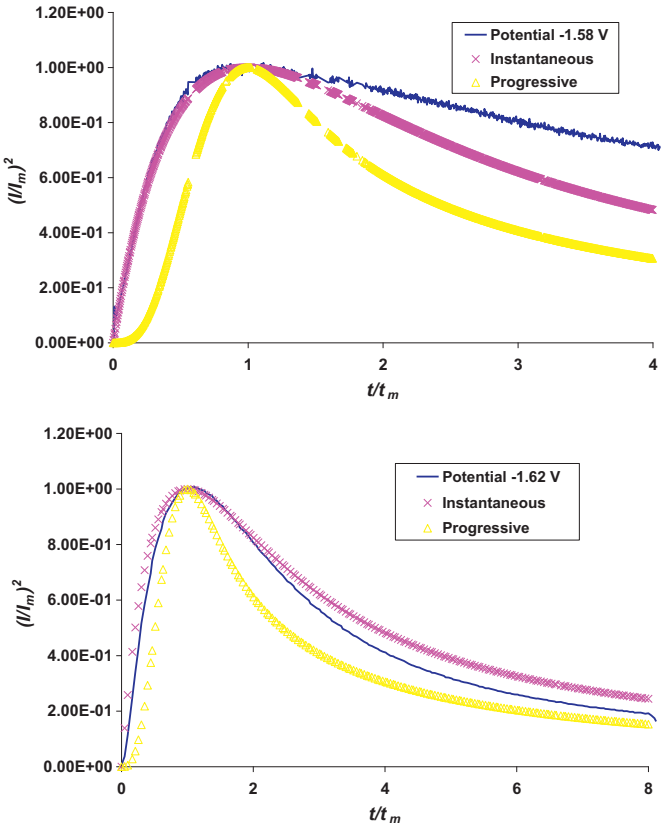


**Fig. 5.** Normalised experimental current–time plots at −1.58 V and −1.62 V for Zn electrodeposition in 0.25 M $Na(CH_3SO_3)$ containing $1.0 \times 10^{-3}$ M $Zn^{2+}$ at 27 °C on Type I (PVDF) electrode compared to simulated curves for instantaneous and progressive nucleation.

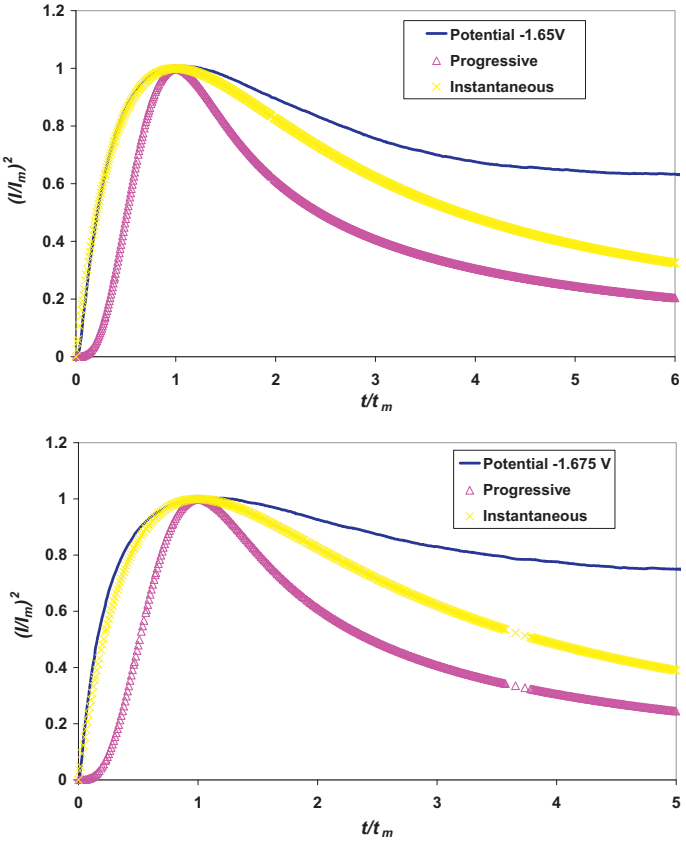


**Fig. 6.** Normalised experimental current–time plots at −1.65 V and −1.675 V for Zn electrodeposition in 1.5 M $Zn^{2+}$ and 5.7 M $CH_3SO_3H$ at 60 °C on glassy carbon electrode compared to simulated curves for instantaneous and progressive nucleation.

data. Fig. 6 shows the corresponding plots of normalized current versus time for a 0.7 M $Zn^{2+}$ in 5.7 M MSA solution. In this case, what is also clearly noticeable is that strong deviations of the experimental data from the theory become increasingly apparent at the more negative potentials. This is due to the increasing contribution to the measured current from the hydrogen evolution reaction (HER). Tables 2 and 3 compare the nuclei density as a function of the potential, as obtained from Eq. (1), for growth of the zinc deposit from a $1.0 \times 10^{-2}$ M $Zn^{2+}$ solution in 0.25 M $Na(CH_3SO_3)$ as well as from 0.7 M $Zn^{2+}$ in MSA solutions on the glassy carbon electrode, respectively. The nuclei density values found for the solution containing $1.0 \times 10^{-2}$ M $Zn^{2+}$ are in a similar range found by Marquez et al. [36] for Ag nucleation on glassy carbon electrodes from silver cyanide solutions. The nuclei density values obtained from the 0.7 M $Zn^{2+}$ solution in MSA (Table 3) are however larger by a factor of 10, indicating an enhanced possibility of forming more compact deposits from this solution. Interestingly, a study of zinc deposition on GC electrodes by Plata-Torres et al. [37] from an ammonium chloride electrolyte revealed the process here to be governed by progressive

**Table 2**
Nuclei density ($cm^{-2}$) as a function of potential for GC and Type I (PVDF) electrodes in $5.0 \times 10^{-3}$ M $Zn^{2+}$ in 0.25 M $Na(CH_3SO_3)$ at 27 °C.

| Potential (V) | Nuclei density ($cm^{-2}$) | |
|---|---|---|
| | Glassy carbon | Type I (PVDF) |
| −1.58 | $5.87 \times 10^5$ | $4.94 \times 10^5$ |
| −1.59 | $6.97 \times 10^5$ | $8.27 \times 10^5$ |
| −1.60 | $8.35 \times 10^5$ | $1.18 \times 10^6$ |
| −1.61 | $4.97 \times 10^6$ | $2.37 \times 10^6$ |
| −1.62 | $4.41 \times 10^6$ | $3.92 \times 10^6$ |
| −1.65 | $8.48 \times 10^6$ | $1.14 \times 10^7$ |

**Table 3**
Nuclei density as a function of potential for glassy carbon electrode in 0.7 M $Zn^{2+}$ and 5.7 M MSA solution at 60 °C.

| Potential (V) | Nuclei density ($cm^{-2}$) |
|---|---|
| −1.6 | $6.80 \times 10^6$ |
| −1.625 | $1.23 \times 10^7$ |
| −1.65 | $1.93 \times 10^7$ |
| −1.675 | $2.52 \times 10^7$ |
| −1.70 | $3.94 \times 10^7$ |
| −1.725 | $4.45 \times 10^7$ |
| −1.75 | $4.95 \times 10^7$ |
| −1.80 | $9.12 \times 10^7$ |

nucleation with initial nuclei densities as low $3.9 \times 10^3$ $cm^{-2}$, thus emphasising the important role played by the counter ions in the adsorption, complexation and transport of the depositing species.

One of the key questions to be answered from the study is how effective are these carbon materials as the negative electrode in the zinc–cerium flow battery. In this respect therefore, the stability of the electrode to repeated zinc deposition and dissolution was determined under a variety of test conditions. Charging and discharging were carried out using current densities in the range of 25 mA $cm^{-2}$ to 250 mA $cm^{-2}$ for different charging periods from 60 s to 2400 s with various electrode rotation frequencies corresponding to Reynolds number, *Re* in the range 50–400. Typical charge discharge curves obtained from the study are shown in Fig. 7(a) for applied current densities of 50 mA $cm^{-2}$ and 25 mA $cm^{-2}$ at an electrode rotation rate of 10 Hz (3770 rpm). It can be seen that apart from the first cycle at 50 mA $cm^{-2}$, the electrode potential during charging quickly attained stable values of −1.52 and −1.82 V at charging current densities of 25 mA $cm^{-2}$ and 50 mA $cm^{-2}$, respectively, over the 60 s duration. The overpotential for charging was thus −0.38 V at 50 mA $cm^{-2}$ whereas at 25 mA $cm^{-2}$, this was reduced to only −0.18 V. Following the

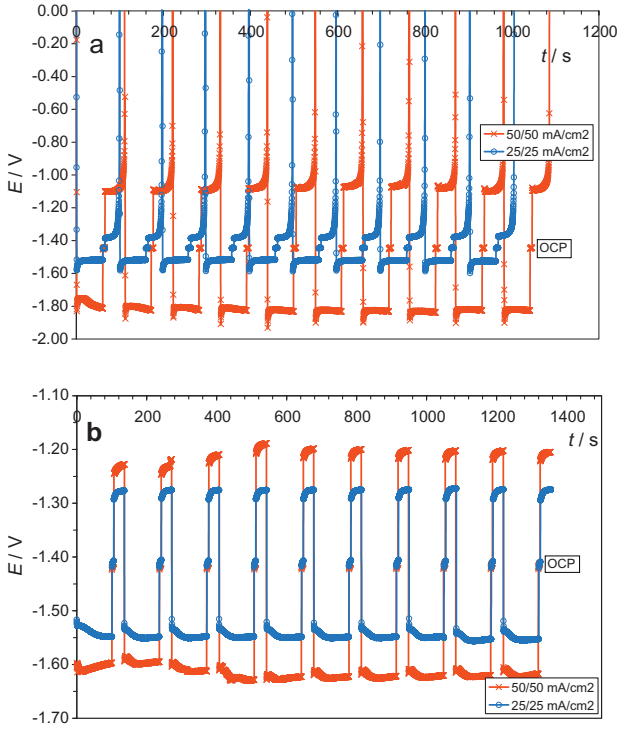


**Fig. 7.** Voltage–time responses to galvanostatic charge/discharge cycles at 25 (–∀–) and 50 mA $cm^{-2}$ (–×–) for Type II (HDPE) electrode in 1.5 M $Zn^{2+}$ and 5.7 M $CH_3SO_3H$ solution at 60 °C and 20 Hz (7400 rpm). (a) Full discharge after charging time of 60 s; (b) partial discharge (charge 100 s/discharge 30 s).

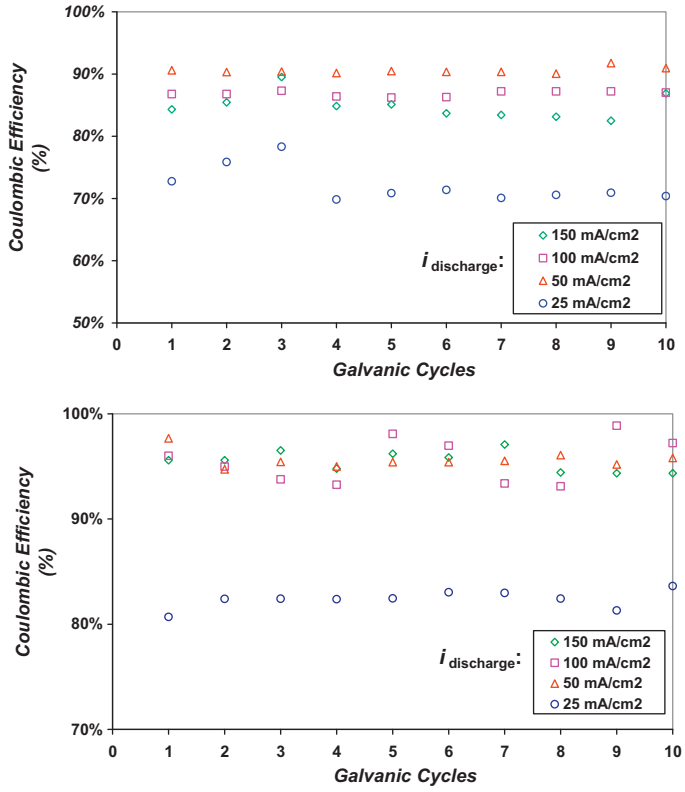


**Fig. 8.** Effect of discharge current density on the coulombic efficiency for Type I (PVDF) electrode in 1.5 M $Zn^{2+}$ and 5.7 M $CH_3SO_3H$ solution at 60 °C and 10 Hz (3700 rpm). Charge time = 300 s at −50 mA $cm^{-2}$.

charging, the electrode was switched to open circuit for 5 s prior to application of the discharge current. This open circuit potential (OCP), of −1.44 V, does not alter with cycling and represents the reversible potential of the zinc deposit in contact with the 1.5 M $Zn^{2+}$ solution. On application of a discharge current density of 50 mA $cm^{-2}$, the voltage falls immediately to a value of −1.1 V whereas at 25 mA $cm^{-2}$, the corresponding potential was −1.38 V. At both these discharge current densities, the potential decreases slightly as the zinc is anodically dissolved back into solution and when all the zinc is exhausted from the electrode surface, the electrode potential jumps sharply towards positive values and the next charging cycle is then imposed. The coulombic efficiency reported here is evaluated simply as ratio of the anodic to cathodic charge consumed in these two events. Fig. 7(b) shows the charge/discharge cycles in which some of the zinc deposit is deliberately left on the carbon substrate prior to the next charging step. It is worth noting that the charging potential here is significantly affected by the presence of the surface zinc, rising to only −1.61 V ($\eta$ = −0.17 V) at 50 mA $cm^{-2}$ and −1.53 V ($\eta$ = −0.09 V) compared to the data in Fig. 7(a), indicating the elimination of the nucleation overpotential for zinc deposition on the carbon substrate. This will greatly assist the voltage and subsequently, energy efficiency of the process. The variation of the anodic discharge potential on the presence of the underlying zinc layer however is less clear. The dissolution process at 50 mA $cm^{-2}$ again appears to occur much more readily on the substrate with a preformed zinc layer, with a lower discharge potential (−1.22 V) recorded compared to that for zinc deposited on the bare carbon substrate (−1.06 V). However, at 25 mA $cm^{-2}$, the discharge potential for the electrode with preformed zinc is −1.29 V compared to −1.38 V for zinc deposited on the bare carbon substrate. This would suggest that at this lower current density, there is some physical and/or morphological mismatch of the newly deposited zinc with respect to the zinc already on the substrate sur-

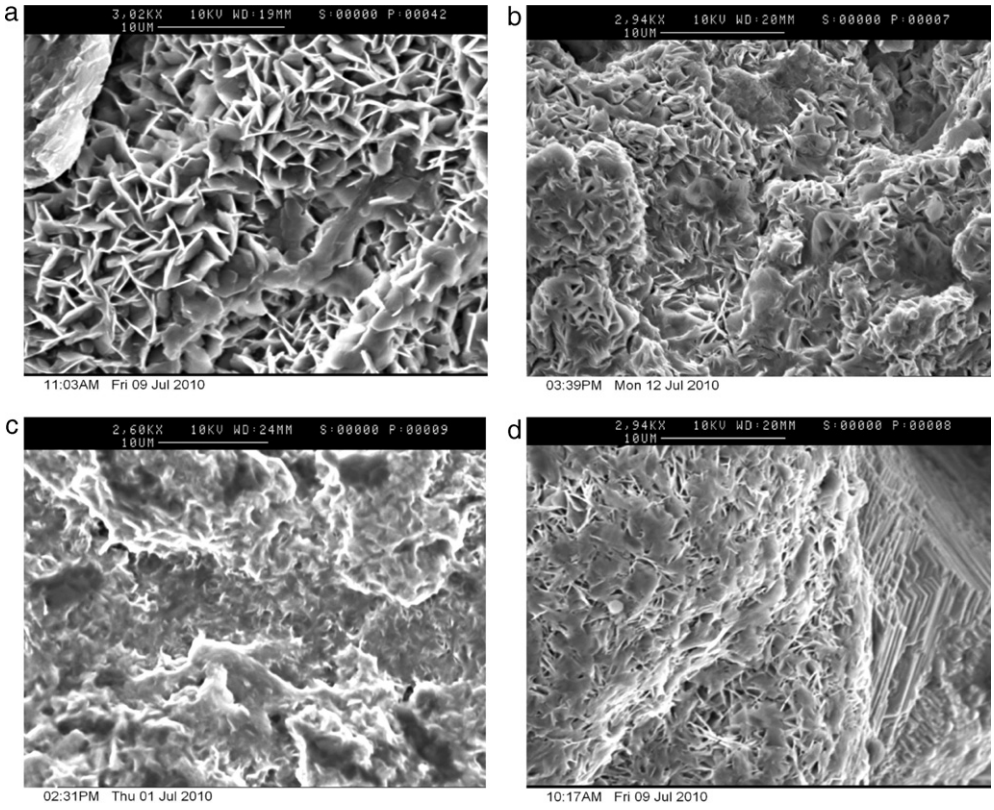


**Fig. 9.** SEM micrographs of Zn deposits in 1.5 M $Zn^{2+}$ and 5.7 M $CH_3SO_3H$ solution at 60 °C for (a) Type II (HDPE) after 120 s deposition, (b) after 2400 s (c) Type I (PVDF) after 120 s deposition and (d) after 2400 s.

face, which has led to an increase in the resistance of the layer and so to a greater discharge overpotential.

Several galvanostatic charge/discharge cycles at −50 mA cm$^{-2}$ (300 s)/50 mA cm$^{-2}$ were conducted on these carbon based electrodes and the coulombic efficiencies, $Q_{eff}$ were evaluated. The plot of the coulombic efficiency $Q_{eff}$ as a function of number of charge–discharge cycles at different current densities is shown in Fig. 8 for the Type I (PVDF) electrode material. The dependence is found not to be very significant for discharge current densities greater than 50 mA cm$^{-2}$. However, at 25 mA cm$^{-2}$, $Q_{eff}$ is lowered to ~80%. In contrast, the corresponding change for the Type II (HDPE) electrode is from 90% at 100 mA cm$^{-2}$ to 70% at 25 mA cm$^{-2}$. This dependence on $i_{discharge}$ must stem from a decreasing competition at high discharge currents from the corrosion of the zinc in the acid solution. It does also point out though that over the time scale of these experiments, corrosion is not a serious issue even at the lowest of the current densities employed for the PVDF electrode. One possible explanation for the difference in $Q_{eff}$ is the increased hydrophobicity of the composite due to the presence of the –C–F bond in the PVDF compared to the –C–H bond in the HDPE polymer. In the strong acidic electrolyte employed here, it is very likely that the HDPE layer may undergo a delamination process leading to a weakening of the binding properties of the polymer and so to a degradation in the structure of the composite electrode. This naturally affects the morphology of the Zn deposited on the materials. This is borne out by the SEM micrographs (Fig. 9) of the zinc deposits on the electrode surfaces after different charging periods and cycling times. More compact deposits are obtained for the PVDF based composite electrode following charging at −50 mA cm$^{-2}$ for 120 s at 10 Hz (3700 rpm) and 60 °C.

The dependence of $Q_{eff}$ on the duration of the charging period is shown in Fig. 10. The trend here is again clearly displayed for the Type I electrode where the shortest deposition times gives the highest $Q_{eff}$ of ~95% and the longest deposition time of 2400 s reduces $Q_{eff}$ to ~70%. For the Type II (HDPE) electrode, the corresponding variation in $Q_{eff}$ was greater, with the efficiency decreasing to around 65% for the longest deposition time. These, along with the SEM micrographs of Fig. 9, suggest that the stability of the deposits is much poorer on the Type III foil (and Type II surfaces) than on the Type I PVDF electrode and increasing the deposition time simply exacerbates this condition.

The effect of electrode rotation rate on $Q_{eff}$ is less clear, as can be gleaned from the data of Fig. 11. The majority of the galvanic cycles conducted at lower rotation rates (6-8 Hz) showed a decrease in $Q_{eff}$ in the range of ~5 to 15% for all of the carbon materials. The low efficiencies could be due to bubble formation occurring during both charge and discharge periods mainly because of the hydrogen evolution reaction with insufficient flow velocity to remove the bubbles from the electrode surface. At higher angular velocities (10–15 Hz), there appears to be very little dependence on this parameter indicating that mass transport of the electrode species does not have a major impact on the deposition/dissolution rates, at least over the solution flow and deposition rates examined here. This can be explained as the deposition reaction using the constant current density ranges employed in this study is well below the mass transport limiting current density of the zinc ion concentration (1.5 M) which can be readily evaluated as 306 mA cm$^{-2}$ at a rotation rate of 10 Hz. At 20 Hz, the efficiency is significantly lowered and this may be attributed to the shearing effect of the solution flow on any loosely adhered deposit particles.

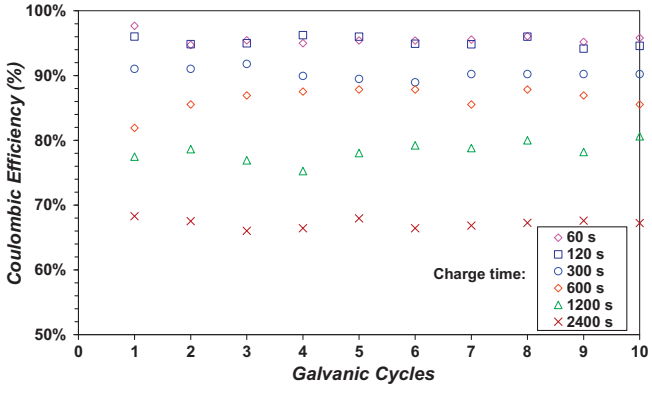


**Fig. 10.** Effect of charging times on the coulombic efficiency for Type I (PVDF) electrode in 1.5 M $Zn^{2+}$ and 5.7 M $CH_3SO_3H$ solution at 60 °C and 10 Hz (3700 rpm). Charge at −50 mA cm$^{-2}$/discharge at 50 mA cm$^{-2}$.

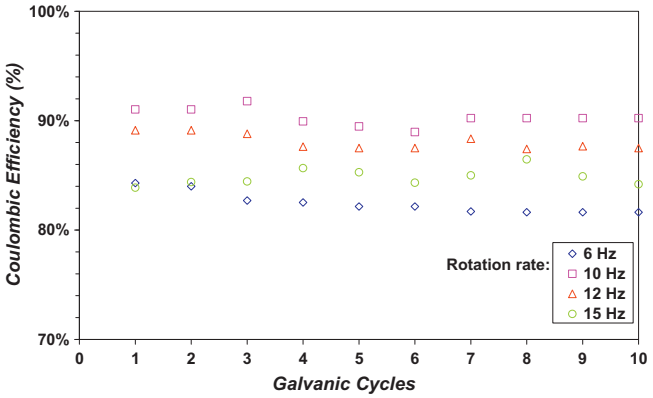


**Fig. 11.** Effect of electrode rotation rate on the coulombic efficiency for Type I (PVDF) electrode in 1.5 M $Zn^{2+}$ and 5.7 M $CH_3SO_3H$ solution at 60 °C. Charge at −50 mA cm$^{-2}$/discharge at 50 mA cm$^{-2}$.

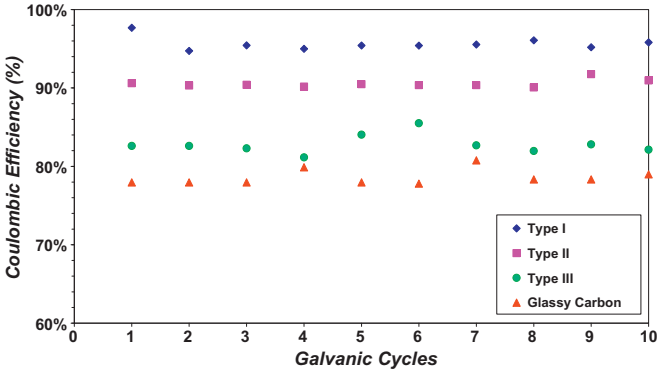


**Fig. 12.** Comparison of $Q_{eff}$ for different composite material electrodes in 1.5 M $Zn^{2+}$ and 5.7 M $CH_3SO_3H$ solution at 60 °C and 10 Hz (3700 rpm). Charge time = 300 s at −50 mA cm$^{-2}$. Discharge: 50 mA cm$^{-2}$.

Fig. 12 compares the different electrode material performances directly. Clearly, the PVDF based electrode shows the best performance of all the electrodes under the conditions examined here. Furthermore, this composite material also exhibited the greatest long term stability to cycling, with no deterioration observed in $Q_{eff}$ or in the physical structure of the electrode surface even after ~200 cycles. This is in contrast to both the Type II HDPE and Type III foil electrodes which, as noted above, degraded substantially after 70 cycles.

## 4. Conclusions

The zinc deposition process from the methane sulfonic acid electrolyte appears to follow the instantaneous nucleation route, with high nuclei densities (~$10^7$ cm$^{-2}$) obtained from the 0.7 M zinc solution in this medium. This enables more compact zinc deposits

to be formed on the composite materials during the galvanostatic charging stage. Low charge and discharge overpotentials are obtained for the zinc deposition/dissolution reaction on the carbon substrates but their dependence on current density, particularly for the discharge process, is also found to be affected by the presence or absence of a preformed zinc layer on the carbon substrate. The highest charge/discharge coulombic efficiencies (~95%) are found at the highest discharge current densities (200 mA $cm^{-2}$) employed in the study but this falls with increased charging period. Prolonged zinc charging–discharging cycling on the composite materials revealed that whereas the PVDF-based electrode exhibited no loss in efficiency with cycling, a drastic reduction was observed for the Type II HDPE-based and Type III foil electrodes which were accompanied by the physical deterioration in the electrode surface.

## Acknowledgements

The authors are grateful to the Scottish Funding Council and to the University of Strathclyde for the provision of a SPIRIT Industry Ph.D. studentship to G.N.

## References

[1] M. Skyllas-Kazacos, M. Rychick, R. Robins, All-Vanadium Redox Battery, US Patent 4,786,567 (November 1988).
[2] M. Skyllas-Kazacos, D. Kasherman, D.R. Hong, M. Kazacos, J. Power Sources 35 (1991) 399.
[3] T. Mohammadi, M. Kyllas-Kazacos, J. Power Sources 63 (1996) 179.
[4] A. Price, S. Bartley, S. Male, G. Cooley, Power Eng. J 13 (3) (1999) 122.
[5] A. Price, S. Male, M. Kleimaier, VDI Berichte 1734 (2002) 47.
[6] M.A. Climent, P. Garces, M. Lopez-Segura, A. Aldaz, An. Quim. 83 (1987) 12.
[7] N.H. Hagedorn, L.J. Thaller, Design Flexibility of Redox Flow Systems NASA TM-82854, DOE/NASA/12726-16 (1982).
[8] M. López-Atalaya, G. Codina, J.R. Pérez, J.L. Vázquez, A. Aldaz, J. Power Sources 39 (1992) 147.
[9] M. Skyllas-Kazacos, J. Power Sources 124 (2003) 299.
[10] V-Fuel Pty. Ltd. <URL: http://www.vfuel.com.au/index.htm>, 2010 (accessed 20.08.10).
[11] Cellstrom GmbH <URL: http://www.cellstrom.com/index.php?id=17&L=1>, 2010 (accessed 20.08.10).
[12] RE-Fuel <URL: http://www.refueltec.com/>, 2010 (accessed 20.08.10).
[13] Cellennium (Thailand) Co. Ltd. <URL: http://www.vanadiumbattery.com/>, 2010 (accessed 20.08.10).
[14] Prudent Energy <URL: http://www.pdenergy.com/>, 2010 (accessed 20.08.10).
[15] Primus Power <URL: http://www.primuspower.com/index.html>, 2010 (accessed 20.08.10).
[16] M. Bartolozzi, J. Power Sources 27 (1989) 219.
[17] C. Ponce de León, A. Frías-Ferrer, J. González-García, D.A. Szánto, F.C. Walsh, J. Power Sources 160 (1) (2006) 716–732.
[18] H.S. Lim, A.M. Lackner, R.C. Knechtli, J. Electrochem. Soc. 134 (1989) 2725.
[19] R.J. Bellows, D.J. Eustace, P. Grimes, J.A. Shropshire, H.C. Tsien, A.F. Venero, in: J. Thompson (Ed.), Power Sources, vol. 7, Academic, London, 1979.
[20] P.C. Butler, J. Chamberlin, R.P. Clark, Ext. Abstr. No. 16, vol. 83–2, Electrochem. Soc., Pennington, New Jersy, 1983, p. 25.
[21] B.D. Brummet, R.D. Clubb, C.J. Warde, J. Electrochem. Soc. 130 (1983) C332.
[22] A. Hazza, D. Pletcher, R. Wills, Phys. Chem. Chem. Phys. 6 (2004) 1773.
[23] D. Pletcher, R. Wills, J. Power Sources 149 (2005) 103–111.
[24] J. McBreen, J. Electroanal. Chem. 168 (1984) 415.
[25] RedFlow <URL: http://www.redflow.com.au/>, 2010 (accessed 20.08.10).
[26] ZBB Energy Corporation <URL: http://www.zbbenergy.com/>, 2010 (accessed 20.08.10).
[27] Plurion Limited <URL: http://plurion.co.uk/>, 2010 (accessed 20.08.10).
[28] C.T.J. Low, F.C. Walsh, Surf. Coat. Technol. 202 (2008) 1339–1349.
[29] V.G. Levich, Physicochemical Hydrodynamics, Prentice Hall, New Jersey, 1962.
[30] J. Koutecky, V.G. Levich, Zhurnal Fizicheskoi Khimii 32 (1958) 1565.
[31] S. Treimer, A. Tang, D.C. Johnson, Electroanalysis 14 (2002) 165.
[32] W.E. Price, H. Weingärtner, J. Phys. Chem. 95 (1991) 8933.
[33] D. Pletcher, F.C. Walsh, Industrial Electrochemistry, Blackie Academic and Professional, London, 1993.
[34] B.R. Scharifker, J. Mostany, M. Palomar-Pardavé, I. Gonzalez, J. Electrochem. Soc. 146 (1999) 1005.
[35] B.R. Scharifker, J. Mostany, J. Electroanal. Chem. 177 (1984) 13.
[36] K. Marquez, G. Staikov, J.W. Schultze, Electrochim. Acta 48 (2003) 875–882.
[37] M. Plata-Torres, S.L. Olvera-Vázquez, C. Ramírez-Rodríguez, H.J. Dorantes-Rosales, E.M. Aree-Estrada, ECS Trans. 3 (2007) 25.